applied sciences

MDPI

Article

Predictive Hybrid Model for Process Optimization and Chatter Control in Tandem Cold-Rolling

Anastasia Mikhaylyuk [1], Gianluca Bazzaro [2] and Alessandro Gasparetto [1,*]

[1] Polytechnic Department of Engineering and Architecture (DPIA), University of Udine, 33100 Udine, Italy; mikhaylyuk.anastasia@spes.uniud.it
[2] Danieli & C. Officine Meccaniche S.p.A., 33042 Buttrio, Italy; g.bazzaro@danieli.it
* Correspondence: alessandro.gasparetto@uniud.it

Featured Application

The proposed hybrid model provides a predictive tool for chatter prevision and process optimization in multi-stand cold rolling mills. It enables the identification of stability margins and supports adaptive control strategies for high-speed rolling operations.

Abstract

Chatter is a self-excited vibration that limits productivity, accelerates roll wear and compromises strip surface quality in high-speed tandem cold-rolling. This work presents a predictive hybrid model that couples the strip-deformation physics to the structural dynamics of a five-stand, 4-high mill, providing a fast decision tool for process optimization and real-time control. The model represents each stand as a four-degree-of-freedom mass–spring–damper system whose parameters are extracted from manufacturing automation datasheets and roll-gap sensing. Linearization about the nominal point yields analytical sensitivity matrices that close the electromechanical loop; the delay between stands is also included in the model. Implemented in MATLAB/Simulink, the computational model, based on data provided by Danieli & C. Officine Meccaniche S.p.A., reproduces the onset of chatter for two types of steel. The framework therefore supports automation-ready scheduling, active vibration mitigation and design-space exploration for next-generation mechatronic cold-rolling systems.

Keywords: chatter; cold rolling; process optimization; hybrid modeling; manufacturing automation; mechatronics

Academic Editor: Augusto Ferrante

Received: 18 December 2025
Revised: 16 January 2026
Accepted: 21 January 2026
Published: 26 January 2026

1. Introduction

Cold rolling (Figure 1) is a cornerstone of modern manufacturing automation, converting hot strip into high-precision sheet for automotive, appliance, and energy markets. It is a metal forming process in which a metallic strip is passed between rotating rolls to reduce its thickness and improve its mechanical properties. The process, carried out below the recrystallization temperature, provides excellent dimensional accuracy and surface quality.

When the line speed exceeds approximately 800 m/min, the process may enter a regenerative, self-excited regime known as "third-octave chatter" (80–160 Hz), which degrades surface finish, accelerates roll wear, and forces conservative scheduling. Because this phenomenon results from the tight interaction between process forces, roll-stack flexibility, hydraulic actuators, and drive control systems, it must be addressed from an integrated mechatronic perspective that combines mechanics, sensing, and computational technologies.

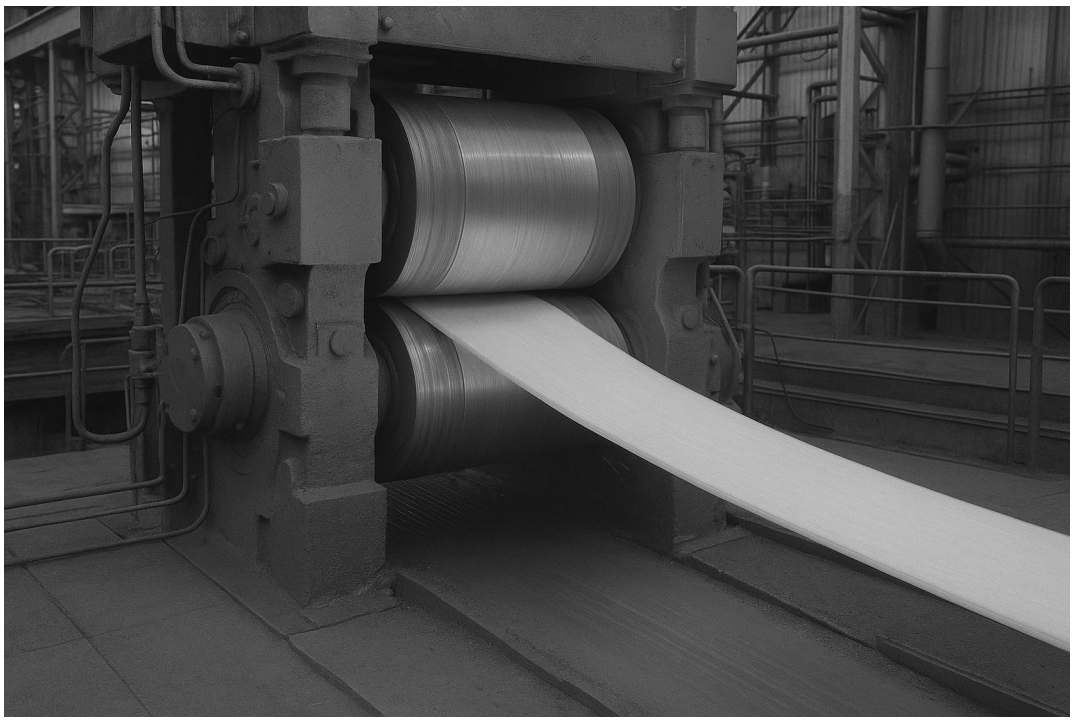

Figure 1. Cold-rolling process (homogeneous view). A strip of entry thickness h_1 is reduced to h_2 while passing through the workroll gap; upstream and downstream tensions act on the strip, and a neutral section develops along the contact arc.

The analytical foundations of rolling were laid by von Kármán [1] and Orowan [2]; Bland and Ford [3,4] later introduced the influence of strip tension and elastic compression, producing force predictions suitable for online optimization. The theory of rolling was further developed in [5–11]. Subsequent research shifted attention to vibration: Tlusty [12], Yun [13], Yun et al. [14–17] and Tamiya et al. [18] linked operating parameters to chatter onset, while Hu and Ehmann [19] formalized linear stability analysis. Experimental studies by Kimura and Sodani [20] highlighted the role of negative strip damping and mode coupling between adjacent stands. More recent contributions to chatter analysis can be found in [21–29].

Despite these advances, most industrial mills still rely on trial-and-error to avoid chatter, leaving substantial room for systematic optimization. This paper develops a predictive process–structure model that (i) retains the essential physics of strip deformation and roll flattening, (ii) captures the dominant structural modes with minimal state order, and (iii) is sufficiently lightweight for frequency-domain design and closed-loop implementation.

The paper is organized as follows: Section 2 introduces the process model; Section 3 develops the chatter model and the associated stability analysis; Section 4 presents the industrial case study, based on data provided by Danieli & C. Officine Meccaniche S.p.A., and numerical results; finally, Section 5 provides conclusions.

The methodology proposed in this work can be extended to any type of cold rolling mill plants, provided that an experimental campaign aimed at identifying the parameters is carried out.

2. Model of the Process

In this section, a homogeneous model [19] of flat cold rolling is formulated. By homogeneous, we mean that the strip and the work rolls are treated as continuous media with spatially uniform, effective properties over the contact arc. Microstructural heterogeneities are not resolved explicitly; the strip is assumed isotropic under plane–strain conditions,

and the roll-stack elasticity is represented by equivalent compliances. This abstraction yields compact relations for pressures, tractions and kinematics, which are later linearized around a nominal operating point for stability analysis.

The model of the coupled strip–roll mechanics that governs force transmission in cold rolling is presented here. We first introduce the notation used throughout the model; variables and units are summarized in Table 1. The geometry of the process is shown in Figure 2.

Table 1. Symbols and definitions used in the homogeneous process model.

Symbol	Description	Unit
h_1, h_2	Strip thickness at the entry/exit of the roll gap	m
h_n	Strip thickness at the neutral point	m
h_c	Strip thickness measured along the roll-bite centerline	m
R	Nominal work-roll radius	m
R'	Deformed (Hitchcock) roll radius	m
l_{arc}	Contact-arc length	m
x_1, x_2	Entry/exit coordinates of the contact	m
x_n	Neutral-point coordinate along the arc	m
x_c	Coordinate of the roll-bite centerline position	m
φ_n	Neutral angle in the roll angular domain	rad
u_1, u_2, u_n	Strip surface speeds at entry/exit and at the neutral point	m s^{-1}
v_r	Roll peripheral speed	m s^{-1}
μ	Friction coefficient (empirical)	-
σ_1, σ_2	Upstream/downstream strip stress (true tension)	MPa
$k_f, k_{f,I}, k_{f,m}$	Flow stress (sectional and mean values)	MPa
ε	True thickness strain	-
w_{wr}	Work-roll angular speed	rad s^{-1}
W_{strip}	Strip width	m
F_y	Vertical component of roll force	N
F_x	Horizontal component of roll force	N
f_y	Vertical component of force per unit width	N m^{-1}
f_x	Horizontal component of force per unit width	N m^{-1}
C_h	Hitchcock compliance term	-
T	Rolling torque	N m

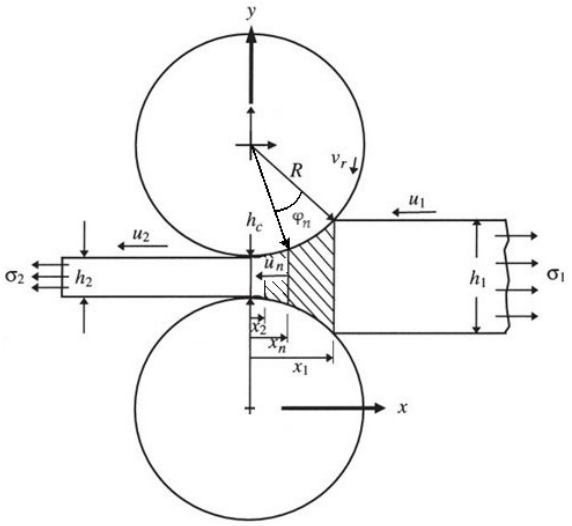

Figure 2. Dynamic model of the cold-rolling process. The neutral point x_n is the position along the contact arc where the strip surface speed equals the roll peripheral speed; φ_n maps that coordinate to the roll angular domain.

The entry coordinate of the contact is computed on the basis of the roll-bite centerline position, of the strip thickness at the entry and exit points, and of the nominal work roll radius, as follows [30]:

$$x_1 = x_c + \sqrt{R(h_1 - h_2) - 0.25(h_1 - h_2)^2} \tag{1}$$

Equation (2) gives the empirical friction factor, whose inverse power dependence on the roll peripheral speed captures the transition from boundary to mixed lubrication in the range $0.4\ \mathrm{m\ s^{-1}} \leq v_r \leq 2.5\ \mathrm{m\ s^{-1}}$:

$$\mu = 1.9526 \cdot (60 \cdot v_r)^{-0.653} \tag{2}$$

A general outlook on friction behavior in cold rolling can be found in [31]; the fitting formula used in this paper Equation (2) has been derived from a data set similar to the one in [32], that Danieli & C. Officine Meccaniche S.p.A acquired through many years in experimental campaigns carried out in several steel cold rolling plants worldwide. These data are part of the industrial know-how of the company and are covered by non-disclosure constraints.

The methodology proposed in this work is still valid if the friction coefficient changes, caused, for example, by the addition of additional lubricating oils or coolants to the rollers and the processed object, as long as the value of the friction coefficient remains within a certain range, as analyzed in [29]. In the case of a change in the friction coefficient, experimental tests should be carried out in order to adjust the curve of the friction coefficient to the new conditions.

The neutral point coordinate is given by:

$$x_n = \sqrt{Rh_2}\tan\left[\frac{\log\left(\frac{k_{f1}-\sigma_1}{k_{f2}-\sigma_2}\right)e^{\left(2\mu\sqrt{\frac{R}{h_2}}\tan^{-1}\left(\frac{l_{arc}}{\sqrt{Rh_2}}\right)\right)}}{4\mu\sqrt{\frac{R}{h_2}}}\right] \tag{3}$$

The velocities u_1 and u_2 at the entry and exit points are given by:

$$u_1 = w_{wr} R \left(1 - \frac{h_n - h_c}{2R}\right)\left(\frac{h_n}{h_1}\right) \tag{4}$$

$$u_2 = w_{wr} R \left(1 - \frac{h_n - h_c}{2R}\right)\left(\frac{h_n}{h_2}\right) \tag{5}$$

The strip thickness at the neutral point can be computed as:

$$h_n = h_2 + \frac{x_n^2}{R} \tag{6}$$

Equation (7) yields the neutral angle in the roll angular domain

$$\varphi_n = x_n \frac{360}{2\pi R} \tag{7}$$

While the velocity at the neutral point is given by:

$$u_n = w_{wr} \cos \varphi_n \tag{8}$$

Equations (3)–(8) define the dynamic model of the cold-rolling process (see Figure 2). In particular, x_n marks the location where the relative tangential velocity vanishes, and φ_n maps that coordinate to the roll angular domain used in the subsequent linearization.

The normal traction $p(x)$ along the roll–strip arc of contact is governed by the equilibrium of the strip elements and by the local strip flow stress. Introducing the entry and exit coordinates x_1 and x_2, the pressure distribution can be written as:

$$p(x) = \begin{cases} \left(k_{f1} - \sigma_1\right) e^{\left(2\mu\sqrt{\frac{R}{h_2}} tan^{-1}\left(\frac{l_{arc}}{\sqrt{Rh_2}}\right)\right)} e^{\left(-2\mu\sqrt{\frac{R}{h_2}} tan^{-1}\left(\frac{x}{\sqrt{Rh_2}}\right)\right)} & x_1 \le x \le x_n \\ \left(k_{f2} - \sigma_2\right) e^{\left(2\mu\sqrt{\frac{R}{h_2}} tan^{-1}\left(\frac{x}{\sqrt{Rh_2}}\right)\right)} & x_n \le x \le x_2 \end{cases} \tag{9}$$

3. Chatter Model and Stability Analysis

Chatter refers to self-excited vibrations arising from the dynamic coupling between the rolling process and the mill structure, typically observed as regenerative oscillations in the roll gap. In this section, the previously derived process model is coupled with a reduced mechanical representation of the mill stands to build a closed-loop chatter framework. This enables frequency-domain evaluation of the conditions under which self-excited vibrations emerge.

3.1. Lumped Mass Models of the Stands

Each mill stand is modeled as a lumped four-degree-of-freedom system comprising work roll, back up roll and housing masses. This abstraction retains the dominant vertical modes while remaining simple enough for frequency domain stability studies.

The stand is modeled as a four-degree-of-freedom lumped mass–spring–damper system (Figure 3).

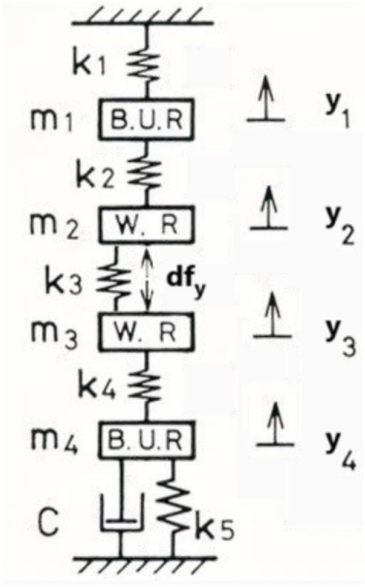

Figure 3. Mechanical model for the vibration analysis of a cage with four degrees of freedom.

To further simplify the structural complexity of rolling mill cages, the system is assumed to be symmetric with respect to the central plane of the rolled strip. This assumption allows for a reduction in the number of degrees of freedom in the model, leading to the formulation of the simplest and most commonly adopted configuration: a single-degree-of-freedom model. Figure 4 shows the equivalent single-degree-of-freedom (1-DOF) representation used for analytical derivations.

$$\mathbf{M}\ddot{\mathbf{y}} + \mathbf{C}\dot{\mathbf{y}} + \mathbf{K}\mathbf{y} = \mathbf{F}_\mathbf{y}(t) \tag{10}$$

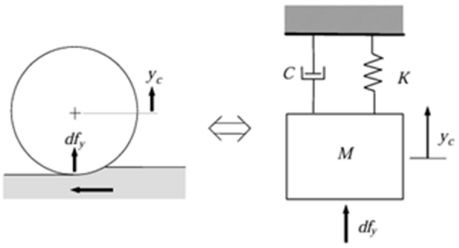

Figure 4. Structural model of the stand with one degree of freedom.

Equation (10) represents the dynamics of the stand, modeled as a four-degree-of-freedom mass–spring–damper system, a configuration introduced by Tlusty [12] for spindle chatter and later adapted to rolling mills. In Equation (10), **y** is the vector of the vertical displacements of the rolls, **M**, **C** and **K** are the mass, damping and stiffness matrices, respectively. The external force $\mathbf{F}_y$ can be defined as the force per unit of length f_y multiplied by the width of the strip W_{strip}:

$$Fy = W_{strip}\, f_y \tag{11}$$

Figure 4 shows the equivalent system with one degree of freedom. The equivalent parameters of the system have been computed according to [33], so as to reduce the number of parameters needed. The assumptions for simplifications can apply to all racks.

3.2. Stiffness and Damping Calculation

Referring to Figure 3, due to the system's symmetry with respect to the central plane, the analysis can be simplified: k_1 and k_5 are equal and represent the stiffness associated with the elastic deformation of the cage, screw blocks, and support cylinder bearings; k_2

and k_4 are also equal and correspond to the elastic contact between the support and work rolls; finally, k_3 denotes the elastic constant of the contact between the work rolls and the material to be rolled.

The elastic constants, as well as the viscous damping coefficients introduced later, were calculated following the method proposed by Yarita and Furukawa et al. [34].

$$k_1 = k_5 = \frac{K}{0.15} \tag{12}$$

$$\frac{1}{k_2} = \frac{1}{k_4} = \frac{\partial D}{\partial F_y} \tag{13}$$

$$\frac{1}{k_3} = \frac{\partial S}{\partial F_y} = -\frac{\partial h2}{\partial F_y} + \frac{\partial E_p}{\partial F_y} = \frac{1}{M_p} + \frac{1}{K_3^*} \tag{14}$$

$$C = \frac{6\eta l_p A_p^2}{\pi R_p \varepsilon_0^3} \tag{15}$$

Here, K is the tandem mill stand, D denotes the reduction in the distance between the centers of the cylinders due to surface flattening, F_y is the vertical force, S is the reduction in thickness and elastic compression of work rolls, h_2 is the exit thickness, Ep is the elastic compression of work rolls, M_p is the equivalent spring constant of strip being rolled, and K_3^* corresponds to the elastic compression constant of the work rolls.

The terms included in the above equations, together with other property of the system, are reported in Tables 2 and 3.

Table 2. Geometrical and material characteristics of the process.

Symbol	Description	Value	Unit
K	Tandem mill stand	4,903,325	N/mm
R_{wr}	Work-roll radius	227.5	mm
R_{br}	Backup-roll radius	700	mm
M_{wr}	Work-roll mass	7700	kg
M_{br}	Backup-roll mass	53,000	kg
E_{roll}	Roll material Poisson's ratio	0.3	-
υ_{roll}	Roll material Yield strength	206,000	MPa
W_{rolls}	Material length	2100	mm
L_{iJ}	Housing span	5200	mm

Table 3. HAGC hydraulic piston characteristics.

Symbol	Description	Value	Unit
ε_0	Clearance between piston and cylinder	0.2	mm
R_p	Piston radius	425	mm
A_p	Effective piston area	526,424	mm^2
l_p	Piston length	111.5	mm
η_{din}	Dynamic viscosity of oil	880×10^{-9}	kg/mm^3

3.3. Development of the Chatter Model

Chatter refers to self-excited vibrations generated by the regenerative coupling between the rolling process and the elastic structure of the mill. During operation, surface modulations produced at one revolution re-enter the deformation zone at the next, modulating the contact pressure and the rolling force. When the energy input from the process

(due to negative damping) exceeds the mechanical dissipation of the stand, oscillations grow exponentially, leading to third-octave chatter [12,31,32].

The dynamic formulation is developed in the Laplace domain. This approach allows the coupling between process and structure to be expressed compactly in the frequency domain, facilitating stability analysis through the Nyquist criteria.

The generalized single-stand chatter model is expressed as follows:

$$\mathbf{y} = \mathbf{G}\,\mathbf{r} \tag{16}$$

Here, $\mathbf{G}$ denotes the transfer function matrix of the chatter model. The explicit representation of its components relies on both the process model (matrix $\mathbf{G_p}$) and the structural dynamics model (matrix $\mathbf{G_s}$). Likewise, we consider the input and output vectors (respectively, $\mathbf{r}$ and $\mathbf{y}$) depending both on the process (vectors $\mathbf{r_p}$ and $\mathbf{y_p}$, respectively) and on the structure (vectors $\mathbf{r_s}$ and $\mathbf{y_s}$, respectively).

The process-related input and output vectors and the corresponding transfer function matrix are as follows:

$$\boldsymbol{r}_p = [d\sigma_1\ d\sigma_2\ dh_1\ 0\ 0\ \ dx_c\ dh_c\ dv_r]^T \tag{17}$$

$$\boldsymbol{y}_p = \left[df_x\ df_y\ dT\ du_1\ du_2\ 0\ 0\ 0\right]^T \tag{18}$$

The elements in Equations (17) and (18) are the variations in the entities defined in Table 1.

The transfer matrix of the process is given by:

$$\boldsymbol{G}_p = \begin{bmatrix} a_{fx,1} & a_{fx,2} & a_{fx,3} & 0 & 0 & a_{fx,4} & a_{fx,5}+a_{fx,6}s & 0 \\ a_{fy,1} & a_{fy,2} & a_{fy,3} & 0 & 0 & a_{fy,4} & a_{fy,5}+a_{fy,6}s & 0 \\ a_{T,1} & a_{T,2} & a_{T,3} & 0 & 0 & a_{T,4} & a_{T,5}+a_{T,6}s & 0 \\ a_{u1,1} & a_{u1,2} & a_{u1,3} & 0 & 0 & a_{u1,4}+a_{u1,5}s & a_{u1,6}+a_{u1,7}s & a_{u1,8} \\ a_{u2,1} & a_{u2,2} & a_{u2,3} & 0 & 0 & a_{u2,4}+a_{u2,5}s & a_{u2,6}+a_{u2,7}s & a_{u2,8} \\ 0 & 0 & 0 & 0 & 0 & 0 & 0 & 0 \\ 0 & 0 & 0 & 0 & 0 & 0 & 0 & 0 \\ 0 & 0 & 0 & 0 & 0 & 0 & 0 & 0 \end{bmatrix} \tag{19}$$

Regarding the structure, the input and output vectors and the corresponding transfer function matrix will be as follows:

$$\boldsymbol{r_s} = \boldsymbol{y_p} = \left[df_x \quad df_y \quad dT \quad du_1 \quad du_2 \quad 0 \quad 0 \quad 0\right]^T \tag{20}$$

$$\boldsymbol{y}_s = \left[0 \quad 0 \quad 0 \quad 0 \quad 0 \quad dx_c \quad dh_c \quad dv_r\right]^T \tag{21}$$

$$\boldsymbol{G}_s = \begin{bmatrix} 0 & 0 & 0 & 0 & 0 & 0 & 0 & 0 \\ 0 & 0 & 0 & 0 & 0 & 0 & 0 & 0 \\ 0 & 0 & 0 & 0 & 0 & 0 & 0 & 0 \\ 0 & 0 & 0 & 0 & 0 & 0 & 0 & 0 \\ 0 & 0 & 0 & 0 & 0 & 0 & 0 & 0 \\ \frac{N_{s,11}(s)}{D_s(s)} & \frac{N_{s,12}(s)}{D_s(s)} & 0 & 0 & 0 & 0 & 0 & 0 \\ \frac{2N_{s,21}(s)}{D_s(s)} & \frac{2N_{s,22}(s)}{D_s(s)} & 0 & 0 & 0 & 0 & 0 & 0 \\ 0 & 0 & \frac{-W_{strip}Rs}{Is^2+Bs+K_r} & 0 & 0 & 0 & 0 & 0 \end{bmatrix} \tag{22}$$

All elements of $\mathbf{G_p}$ are obtained during the linearization process (Appendix A) by approximating the non-linear model, at a nominal operating point, by means of a Taylor series truncated to the first-order terms, so that the coefficients appearing in (A1) through

(A5) are the first-order partial derivatives of the function with respect to the variables on which the function depends, computed at the nominal operating point. The derivation of the terms of the structure's transfer function matrix G_s is presented in Hu et al. [35–37].

3.4. Single-Stand Chatter Model and Stability Analysis

As illustrated in Figure 5, the formulation for determining the single-stand open-loop transfer function matrix is expressed as follows:

$$\mathbf{G}(s) = \mathbf{M}_2(\mathbf{I} + \mathbf{G_s})(\mathbf{I} - \mathbf{G_p}\mathbf{G_s})^{-1}\mathbf{G_p}\mathbf{M}_1 \tag{23}$$

where $\mathbf{I}$ denotes the identity matrix and $\mathbf{M}_1$ and $\mathbf{M}_2$ represent the connection matrices [35].

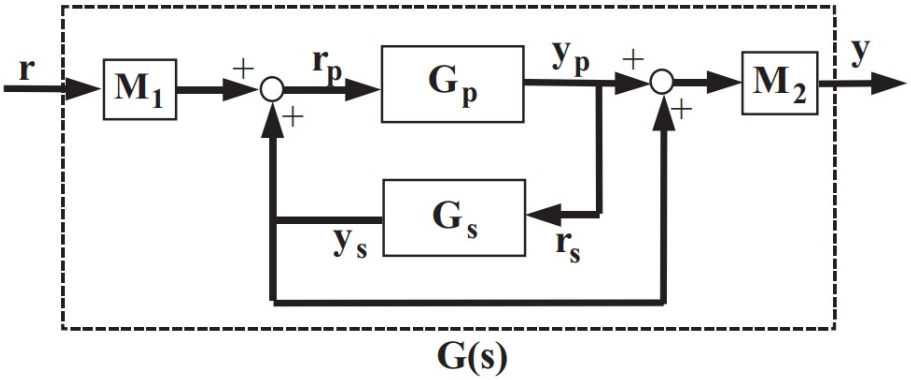

Figure 5. Block diagram of the single-stand chatter model.

Based on the derived linear model, two physical mechanisms leading to undesired vibrations are examined: the matching effect and mode coupling. The matching effect arises from a simple process–structure interaction, offering a relatively high stability margin, and was first introduced by Hu, Zhao, and Ehmann [36]. Conversely, mode coupling results from multiple vibration modes and was initially established in a limited form by Yun et al. [14–16].

The transfer function matrix model allows system analysis via its characteristic equation, where stability requires all roots to have negative real parts; the characteristic equation for (23) is:

$$D(s) = M^2\delta(s)\left(Is^2 + Bs + K_r\right)\left(Ms^2 + C_{x'}s + K_{x'}\right)\left(Ms^2 + C_{y'}s + K_{y'}\right) \tag{24}$$

Here, M denotes the equivalent mass, calculated as the sum of the work roll mass and the backup roll mass; Cx', $Cy\prime$ are the structural damping coefficients along the X and Y axes; Kx', $Ky\prime$ are the spring constants along the X and Y axes (see Figure 6).

δ(s) is a fourth-degree polynomial:

$$\delta(s) = s^4 + a_1s^3 + a_2s^2 + a_3s + a_4 \tag{25}$$

where the coefficients appearing in Equation (25) are defined in Zhao and Ehmann [33].

Equation (24) includes two types of roots: six from the structural dynamic model and four from the combined process–structure model. According to Hu, Zhao, and Ehmann [36], the six roots related to structural dynamics are stable and can be neglected; thus, system stability requires the remaining four roots to have negative real parts.

From the general form of Equation (24), the model matching effect is not immediately evident; referring to Figure 6, considering the case where $\alpha = 0$, the main structural dynamic modes align with the vertical and horizontal directions and become decoupled

into two independent modes. Thus, the stability analysis for the model matching effect reduces to a simple verification.

$$C' = C_{y\prime} - 2W_{strip}a_{fy,6} > 0 \tag{26}$$

$$K' = K_{y\prime} - 2W_{strip}a_{fy,5} > 0 \tag{27}$$

Here, C' denotes the equivalent damping coefficient, and K' represents the equivalent spring constant of the system.

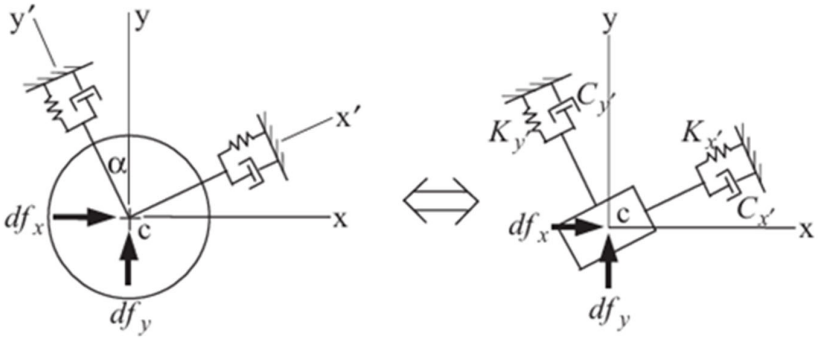

Figure 6. Structural Dynamics Model.

In processes where the tool can oscillate in multiple directions, instability may arise from modal coupling even if each individual direction is stable. Although horizontal oscillations in rolling are minimal, they can still destabilize the system. To analyze this effect, a multidirectional, multimodal structural model is required, and stability is typically assessed using the Routh criterion:

$$\begin{array}{c|ll} s^4 & 1 & a_2 & a_4 \\ s^3 & a_1 & a_3 \\ s^2 & b_1 & b_2 \\ s & c_1 \\ 1 & d_1 \end{array} \tag{28}$$

$$a_1 > 0, \quad b_1 > 0, \quad c_1 > 0, \quad d_1 > 0 \tag{29}$$

In this case, system stability depends on factors influenced by both the process and structural dynamics, but primarily on the angle α and the structural properties along the x' and y' directions (Figure 6).

3.5. Multi-Stand Chatter Model and Stability Analysis

In industrial rolling processes, most mills operate in a tandem configuration, where multiple rolling stands are arranged sequentially to enable continuous thickness reduction. While this setup ensures high efficiency, it also introduces dynamic instabilities, primarily linked to negative damping effects. To analyze these phenomena, the multi-stand chatter model plays a crucial role, as it captures the interaction mechanisms between stands and explains the occurrence of third-octave vibrations during rolling operations.

Considering the strip between stands (i) and (i − 1) (Figure 7), according to Hooke's law, the variation in stress at the entry of stand (i) is proportional to the integral of the difference between the exit speed of stand (i − 1) and the entry speed of stand (i):

$$d\sigma_1 = \frac{E}{L_{i-1}} \int (du_1 - du_{2,i-1})dt \tag{30}$$

$$d\sigma_2 = \frac{E}{L_i}\int (du_{1,i+1} - du_2)dt \tag{31}$$

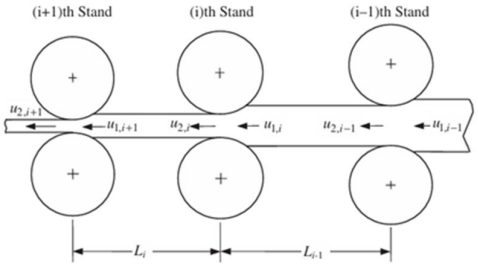

Figure 7. Interrelation of the rolling mill stands.

Here, E represents the Young's modulus of the strip, and L_i denotes the distance between stands i and $i+1$.

For notational convenience, the subscript i has been suppressed for variables pertaining to stand (i).

Another key relation between two consecutive stands concerns how the thickness variation in one stand affects the next. The strip exiting stand (i − 1) reaches the rolling zone of stand (i) after a time delay, defined as follows:

$$\Delta_i = \frac{L_{i-1}}{u_{2,i-1}} \tag{32}$$

Thus, the transfer function that describes the relationship between strip thickness variations at the entry and exit can be expressed as follows:

$$dh_{1,i} = e^{-s\Delta_i} dh_{c,i-1} \tag{33}$$

In Figure 8, the single-stand model of Equation (23) is represented by $G_i(s)$. Upstream and downstream influences are transmitted to Gi(s) through the transport matrix T_i, which defines inter-stand relations. Outputs of the current stand depend on its inputs, and this effect is included in T_i; the input vector for a multi-stand model is defined as follows:

$$\boldsymbol{r_i'} = \begin{bmatrix} du_{2,i-1} & du_{1,i+1} & dh_{c,i-1} \end{bmatrix}^T \tag{34}$$

The transport matrix Ti can be expressed as:

$$\boldsymbol{T}_i = (\boldsymbol{I} + \boldsymbol{H}_i\boldsymbol{G}_i)^{-1}(\boldsymbol{H}_i + \boldsymbol{D}_i) \tag{35}$$

where

$$\boldsymbol{H}_i = \begin{bmatrix} -\frac{E}{L_{i-1}s} & 0 & 0 \\ 0 & \frac{E}{L_i s} & 0 \\ 0 & 0 & 0 \end{bmatrix} \tag{36}$$

$$\boldsymbol{D}_i = \begin{bmatrix} 0 & 0 & 0 \\ 0 & 0 & 0 \\ 0 & 0 & e^{-s\Delta_i} \end{bmatrix} \tag{37}$$

The multi-stand chatter model in Figure 8 can be expressed as:

$$\boldsymbol{G}_i' = \boldsymbol{G}_i\boldsymbol{T}_i = \boldsymbol{G}_i(\boldsymbol{I} + \boldsymbol{H}_i\boldsymbol{G}_i)^{-1}(\boldsymbol{H}_i + \boldsymbol{D}_i) \tag{38}$$

To analyze inter-stand tension effects due to strip speed differences, the multi-stand model is applied, where horizontal roll motion has been assumed negligible compared to vertical motion. The Routh criterion is then applied [37].

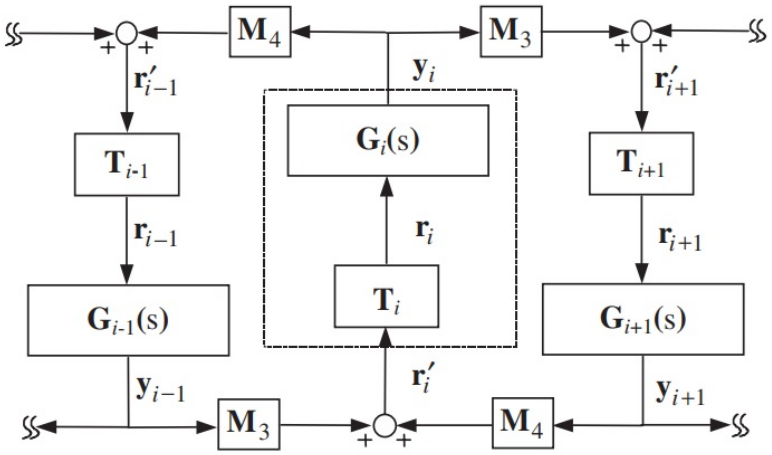

Figure 8. Block diagram of the multi-stand chatter model.

The resulting characteristic equation for the *i*-th stand can be expressed as follows:

$$D_i'(s) = a_0 s^6 + a_1 s^5 + a_2 s^4 + a_3 s^3 + a_4 s^2 + a_5 s + a_6 \tag{39}$$

$$\begin{array}{c|llll} s^6 & a_0 & a_2 & a_4 & a_6 \\ s^5 & a_1 & a_3 & a_5 & \\ s^4 & b_1 & b_2 & b_3 & \\ s^3 & c_1 & c_2 & & \\ s^2 & d_1 & d_2 & & \\ s & e_1 & & & \\ 1 & f_1 & & & \end{array} \tag{40}$$

$$a_1 > 0, \;\; b_1 > 0, \;\; c_1 > 0, \;\; d_1 > 0, \;\; e_1 > 0, \;\; f_1 > 0 \tag{41}$$

4. Results

This section compares the calculated stability boundaries with experimental mill data for two steel grades. Natural frequencies, equivalent stiffnesses, and critical speeds are extracted and tabulated to assess the predictive accuracy of the proposed model.

The hybrid chatter model is applied to the industrial scenario that motivated the research. The study focuses on a five–stand, 4–high tandem cold–rolling mill built by Danieli Group, selected because persistent third–octave chatter has been observed during production runs. Incoming low-carbon strip of 2.5 mm thickness is progressively reduced to final gauges between 0.30 mm and 0.55 mm over five passes, following the reduction schedules listed in Tables 4–7 of this paper. All geometric, inertial and compliance data—roll diameters, stand modulus, HAGC cylinder characteristics and inter-stand spacing—are taken unaltered from the plant datasheet and summarized here in Tables 2 and 3. These measured inputs serve as boundary conditions for the linearized process–structure model, allowing the predicted stability index to be compared directly with the mill's recorded chatter limits.

Table 4. Mechanical properties and parameters for Steel I.

Symbol	Property			Value	Unit
Y_0	Yield strength			780	MPa
$B_{material}$	Work hardening coefficient			50	MPa
n	Strain hardening exponent			0.1	-
E	Young's modulus			198–210 × 10^3	MN/m^2
W_{strip}	Strip width			1450	mm
Stand	**Entry Thickness h_1 [mm]**	**Entry Thickness h_2 [mm]**	**Stress σ_1 [MPa]**	**Stress σ_1 [MPa]**	**Angular Speed w_{wr} [rad/s]**
1	2.5	1.99	98.07	127.49	27.24
2	1.99	1.61	127.49	158.87	33.71
3	1.61	1.32	158.87	171.62	40.86
4	1.32	1.12	171.62	158.87	48.53
5	1.12	1	158.87	37.27	54.13

Table 5. Mechanical properties and parameters for Steel II.

Symbol	Property			Value	Unit
Y_0	Yield strength			280	MPa
$B_{material}$	Work hardening coefficient			160	MPa
n	Strain hardening exponent			0.18	-
E	Young's modulus			190–210 × 10^3	MN/m^2
W_{strip}	Strip width			1450	mm
Stand	**Entry Thickness h_1 [mm]**	**Entry Thickness h_2 [mm]**	**Stress σ_1 [MPa]**	**Stress σ_1 [MPa]**	**Angular Speed w_{wr} [rad/s]**
1	1.8	1.15	98.07	123.56	22.89
2	1.15	0.75	123.56	158.87	35.22
3	0.75	0.52	158.87	176.52	51.04
4	0.52	0.38	176.52	176.52	68.98
5	0.38	0.3	176.52	57.86	87.91

Table 6. Results obtained for Steel I.

Variable	Stand n°1	Stand n°2	Stand n°3	Stand n°4	Stand n°5	Unit
$w_{n,br}$	1138	1135	1128	1119	1108	Hz
$w_{n,wr}$	4569	4549	4507	4442	4366	Hz
v_r	0.6489	0.8031	0.9735	1.1561	1.2896	m/s
μ	0.1787	0.1555	0.1371	0.1226	0.1141	-
k_{fm}	1115	1166	1199	1220	1233	MPa
x_1	0.0108	0.0093	0.0081	0.0067	0.0052	m
x_n	0.0043	0.0043	0.0038	0.0031	0.0023	m
u_1	0.5376	0.6822	0.8361	1.0189	1.1778	m/s
u_2	0.6753	0.8433	1.0197	1.2009	1.3191	m/s
$k_1 = k_5$	32,689	32,689	32,689	32,689	32,689	MN/mm
$k_2 = k_4$	78,103	78,039	76,997	75,302	73,298	MN/mm
k_3	76,540	75,134	73,243	70,597	67,545	MN/mm
C	549.86	549.86	549.86	549.86	549.86	MNs/m
F_y	22.76	22.39	19.75	16.13	12.55	MN

Table 7. Results obtained for Steel II.

Variable	Stand n°1	Stand n°2	Stand n°3	Stand n°4	Stand n°5	Unit
$w_{n,br}$	1178	1179	1162	1148	1135	Hz
$w_{n,wr}$	4833	4839	4715	4616	4519	Hz
v_r	0.5454	0.839	1.216	1.6433	2.0944	m/s
μ	0.2002	0.1511	0.1186	0.0974	0.0831	-
k_{fm}	630.26	649.5	732.19	758.03	774.89	MPa
x_1	0.0122	0.0095	0.0072	0.0056	0.0043	m
x_n	0.0039	0.0041	0.0032	0.0025	0.0018	m
u_1	0.3987	0.602	0.9171	1.291	1.7351	m/s
u_2	0.5772	0.923	1.3227	1.7666	2.1978	m/s
$k_1 = k_5$	32,689	32,689	32,689	32,689	32,689	MN/mm
$k_2 = k_4$	77,334	79,351	76,204	73,677	71,230	MN/mm
k_3	97,205	95,382	89,539	85,044	80,798	MN/mm
C	549.86	549.86	549.86	549.86	549.86	MNs/m
F_y	21.7	27.52	19.84	14.87	11.12	MN

Table 6 summarizes the natural frequencies, process variables and equivalent stiffnesses for Steel I. The rapid strain hardening of the material at higher rolling speeds increases the strip stiffness, which alters the system's natural frequencies and brings them closer to those of the induced vibrations. This phenomenon can be observed through the progressive increase in the mean flow stress value k_{fm} from stand 1 to stand 5.

Analogous data for Steel II are given in Table 7. Owing to its higher work-hardening coefficient of Steel II, the effective flow stress increases more between the first two stands, leading to a steeper stiffness gradient.

In the multi-cage rolling model, the second, third, and fourth cages were selected for detailed analysis. This selection is justified because the first cage does not experience stresses induced by a preceding cage, thereby minimizing instability risks. Conversely, in the fifth and final cage, the material reductions are minimal; thus, despite work hardening, the likelihood of vibration remains low. Literature [20] and experimental evidence indicate that vibrations predominantly occur in intermediate cages and tend to intensify in subsequent stages, amplifying instability effects.

Experimental investigations were conducted to assess system behavior as a function of the working roll's peripheral speed and the friction coefficient. For each material, a speed range was established from 110% down to 50% of the nominal speed, with decrements of 10%. At each speed level, tests were performed considering the friction coefficient, which varied proportionally with speed, as calculated using Equation (2). The coefficient was progressively reduced to the minimum realistic value, avoiding negative values due to their lack of physical significance.

In order to assess the stability of the system, stability diagrams correlating peripheral speed (v_r) and friction coefficient (μ) have been obtained. Moreover, additional plots were developed to illustrate the trend of the stability index Q relative to roll speed.

$$Q = \left|\frac{\partial R}{\partial h}\right| \Delta_i = M_p \Delta_i \tag{42}$$

This index, originally proposed by Kimura, Sodani et al. [20], provides a measure of the system's stability against vibrations. It depends solely on the rolling conditions and is independent of the physical configuration of the mill. An increasing value of the stability index Q indicates a higher tendency of the system to become unstable.

The results presented focus on cages 2–4, which represent critical stages in the rolling process where variations in material properties and system dynamics are most pronounced.

Figure 9 clearly shows that the stability index decreases with the peripheral speed of the working roll.

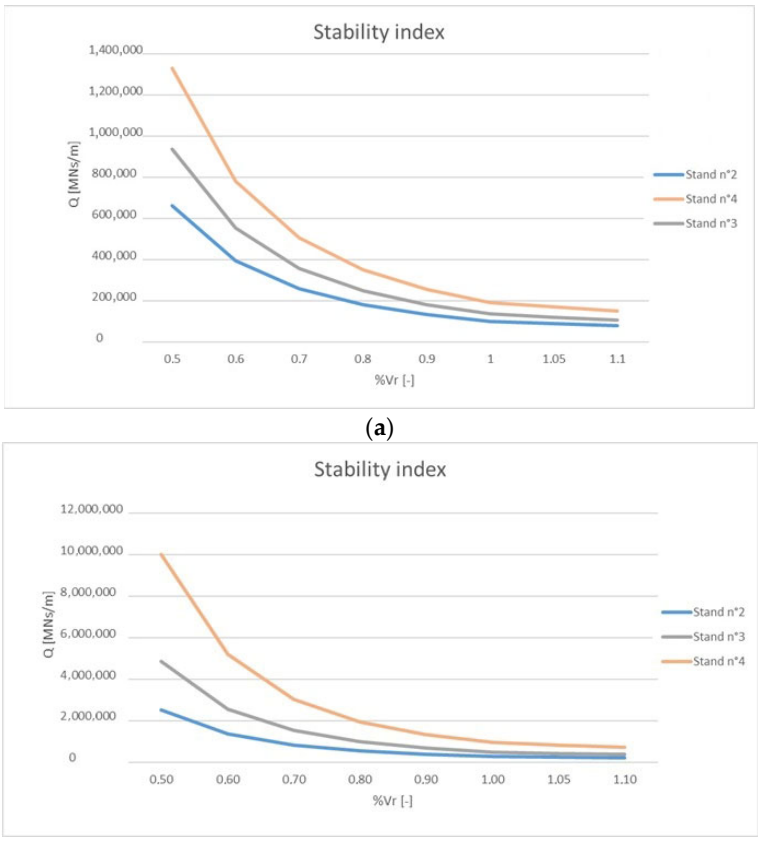

Figure 9. Stability index Q as a function of the work-roll peripheral speed v_r for Steel I (**a**) and Steel II (**b**).

A reduction in rolling speed by approximately 50% from the nominal condition produced an unexpected outcome: rather than improving process stability, the system exhibited signs of increased instability. This behavior can be explained by several mechanisms associated with excessively low rolling speeds in cold rolling operations. At reduced speeds, the friction coefficient between the strip and the rolls tends to increase, leading to irregular force distribution and unpredictable fluctuations. Additionally, the effectiveness of dynamic damping decreases, making the system more sensitive to self-excited vibrations. Low speeds may also alter the natural frequencies of the strip-roll assembly, potentially bringing them closer to excitation frequencies and thereby promoting resonance phenomena.

Conversely, the ability to maintain stability even with a 10% increase in rolling speed above the nominal value confirms that the selected process parameters are well optimized and provide a safety margin against moderate speed variations.

Figures 10 and 11 show a stability analysis for stands 2–4, as a function of two parameters—the peripheral speed and the friction coefficient. The points defined as "unstable" in Figures 10 and 11 are the combination of values of roll peripheral speed and of friction coefficient for which the simulations yield an unstable system (poles with positive real part, or negative stiffness, or negative damping). The stability analysis was performed according to the methodology described by Kimura, Sodani et al. [20]. It can be noticed that instability occurs for low values of the friction coefficient μ.

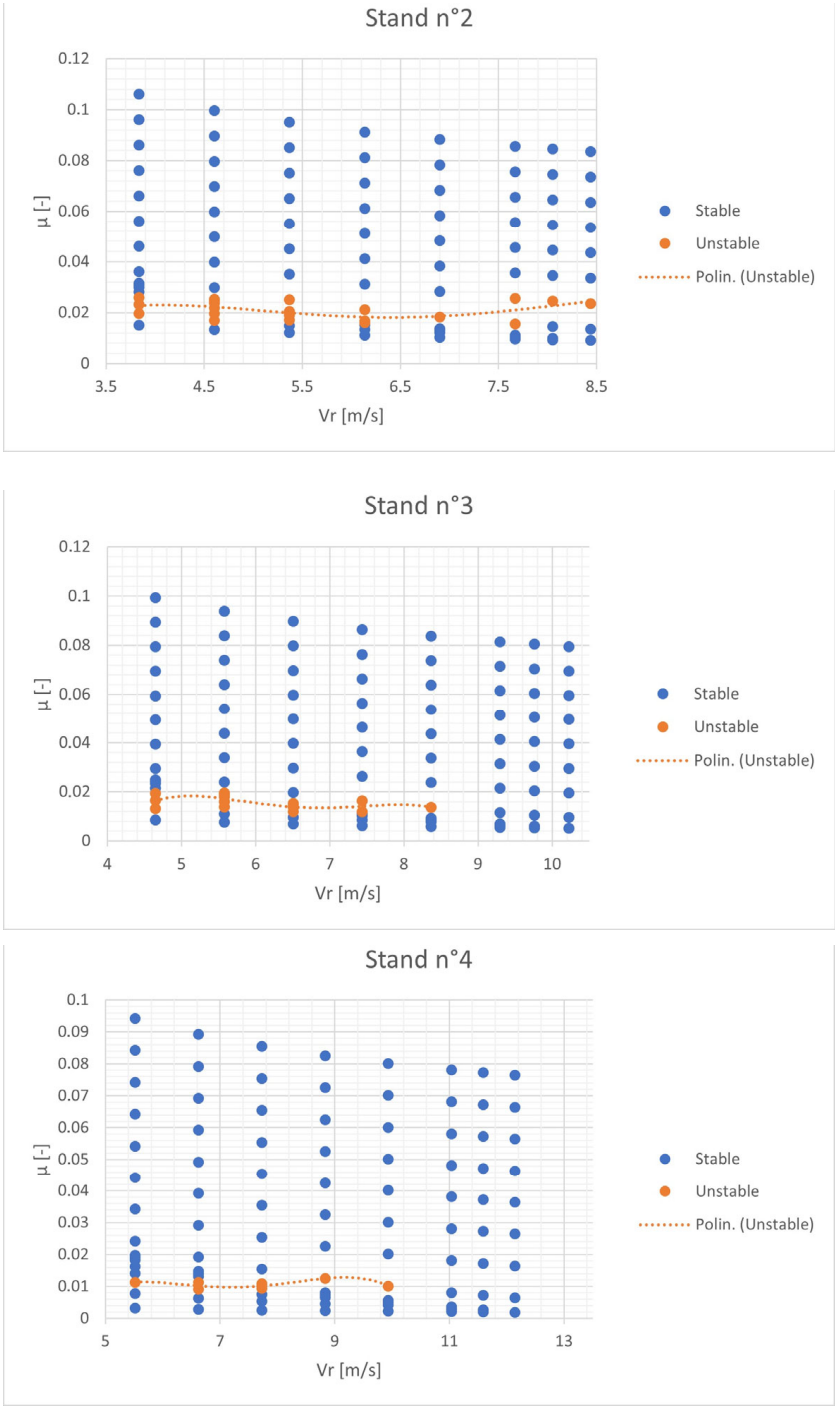

Figure 10. Analysis of stability as a function of the working cylinder peripheral speed and friction coefficient for the second, third, and fourth stands for Steel I.

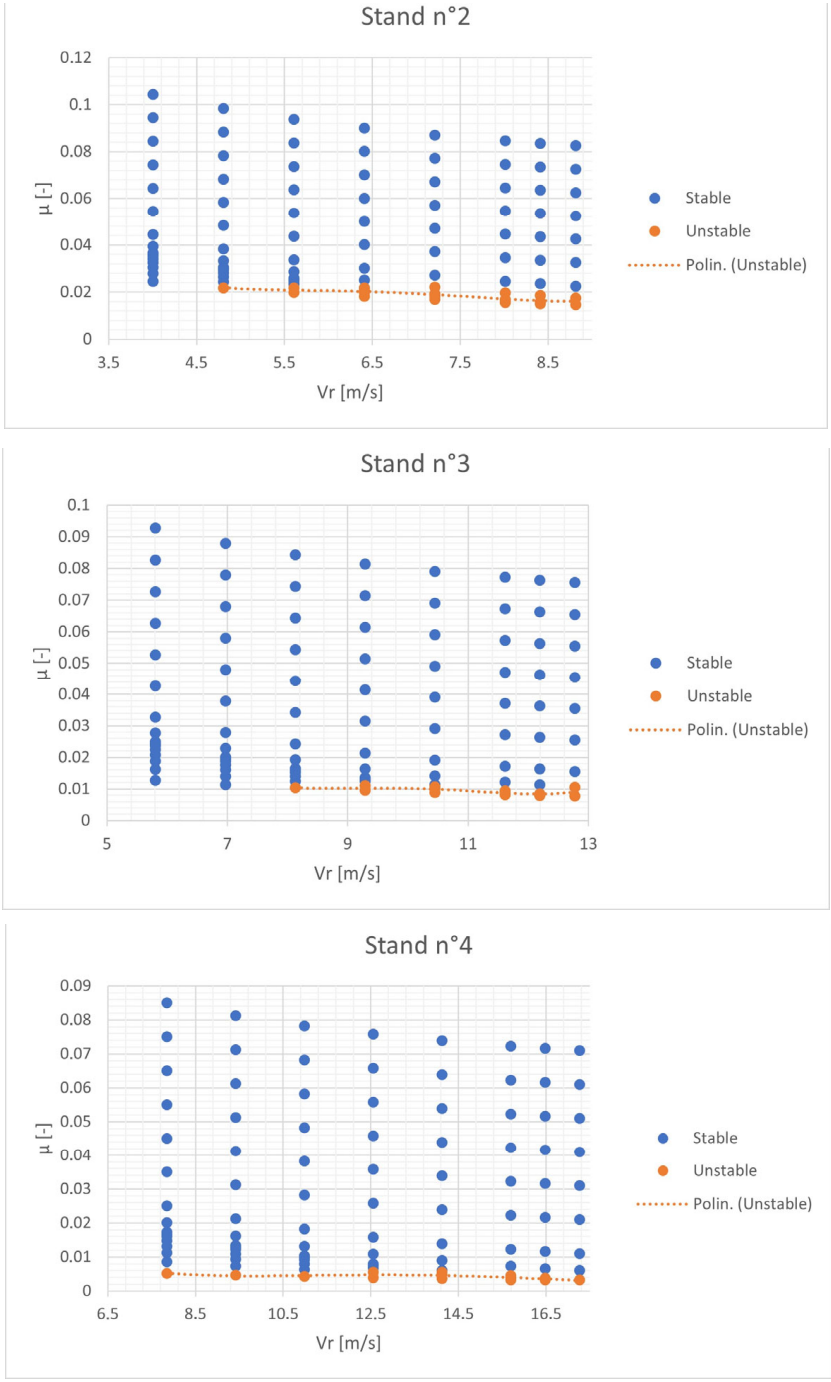

Figure 11. Analysis of stability as a function of the working cylinder peripheral speed and friction coefficient for the second, third, and fourth stands for Steel II.

5. Materials and Methods

During the preparation of this manuscript, the authors used ChatGPT (version 5.2) for the purpose of generating Figure 1. The authors have reviewed and edited the output and take full responsibility for the content of this publication.

6. Conclusions

This work has presented a hybrid process–structure model that links strip-deformation mechanics to stand dynamics, offering a predictive tool for process optimization and vibration control in tandem cold-rolling. By combining von Kármán–Orowan pressure equations [1,2], iterative Hitchcock roll-flattening [17] and a four-degree-of-freedom lumped

stand model, the approach reproduces the experimentally observed onset of third-octave chatter for three low-carbon steels.

The results highlight how friction coefficient, stand stiffness and hydraulic clearances shift the stability boundary, providing quantitative guidelines for roll-speed scheduling and adaptive damping. Because the state-space is compact and implemented in MATLAB/Simulink version R2020a, the model runs fast enough for real-time what-if studies and can be embedded into existing manufacturing-automation and sensing architectures. These features align with the objectives of modern mechatronic system design, where computational technologies are leveraged to maximize throughput while safeguarding product quality.

Author Contributions: Conceptualization, A.M., G.B. and A.G.; methodology, A.M., G.B. and A.G.; software, A.M. and G.B.; validation, A.M. and G.B.; formal analysis, A.M., G.B. and A.G.; investigation, A.M. and G.B.; resources, G.B.; data curation, A.M.; writing—original draft preparation, A.M.; writing—review and editing, A.M. and A.G.; supervision, G.B. and A.G. All authors have read and agreed to the published version of the manuscript.

Funding: This research received no external funding.

Institutional Review Board Statement: Not applicable.

Informed Consent Statement: Not applicable.

Data Availability Statement: Restrictions apply to the availability of these data. Data were obtained from Danieli & C. Officine Meccaniche S.p.A. and are available with the permission of Danieli & C. Officine Meccaniche S.p.A.

Acknowledgments: During the preparation of this manuscript, the authors used ChatGPT (version 5.2) for the purpose of generating Figure 1. The authors have reviewed and edited the output and take full responsibility for the content of this publication.

Conflicts of Interest: Author Gianluca Bazzaro is employed by the Danieli & C. Officine Meccaniche S.p.A. The remaining authors declare that the research was conducted in the absence of any commercial or financial relationships that could be construed as a potential conflict of interest.

Appendix A. Linearization of the Process Model

The nonlinear equations of Section 2 are expanded by a first-order Taylor series around the nominal steady state. The incremental form for a generic output y_i is:

$$dy_i = \left(\frac{\partial y_i}{\partial \sigma_1}\right)_{ss} d\sigma_1 + \left(\frac{\partial y_i}{\partial d\sigma_2}\right)_{ss} d\sigma_2 + \left(\frac{\partial y_i}{\partial h_1}\right)_{ss} dh_1 + \left(\frac{\partial y_i}{\partial h_c}\right)_{ss} dh_c + \left(\frac{\partial y_i}{\partial \dot{h}_c}\right)_{ss} d\dot{h}_c + \left(\frac{\partial y_i}{\partial x_c}\right)_{ss} dx_c + \left(\frac{\partial y_i}{\partial \dot{x}_c}\right)_{ss} d\dot{x}_c + \left(\frac{\partial y_i}{\partial v_r}\right)_{ss} dv_r \quad \text{(A1)}$$

These relations define the state–space model used in Section 3 for the chatter stability analysis.

$$df_y = a_{fy,1} d\sigma_1 + a_{fy,2} d\sigma_2 + a_{fy,3} dh_1 + a_{fy,4} dx_c + a_{fy,5} dh_c + a_{fy,6} dv_r \quad \text{(A2)}$$

$$du_1 = a_{u1,1} d\sigma_1 + a_{u1,2} d\sigma_2 + a_{u1,3} dh_1 + \left(a_{u1,4} + a_{u1,5}\right) dx_c + \left(a_{u1,6} + a_{u1,7}\right) dh_c + a_{u1,8} dv_r \quad \text{(A3)}$$

$$du_2 = a_{u2,1} d\sigma_1 + a_{u2,2} d\sigma_2 + a_{u2,3} dh_1 + \left(a_{u2,4} + a_{u2,5}\right) dx_c + \left(a_{u2,6} + a_{u2,7}\right) dh_c + a_{u2,8} dv_r \quad \text{(A4)}$$

$$\boldsymbol{dT} = \boldsymbol{a_{T,1}} d\sigma_1 + \boldsymbol{a_{T,2}} d\sigma_2 + \boldsymbol{a_{T,3}} \boldsymbol{dh_1} + \boldsymbol{a_{T,4}} \boldsymbol{dx_c} + \boldsymbol{a_{T,5}} \boldsymbol{dh_c} + \boldsymbol{a_{T,6}} \boldsymbol{dv_r} \quad \text{(A5)}$$

References

1. Von Karmàn, T. Beitrag zur Theorie des Walzvorganges. *Z. Angew. Math. Mech.* **1925**, *5*, 139–141. [CrossRef]
2. Orowan, E. The calculation of roll pressure in hot and cold flat rolling. *Proc. Inst. Mech. Eng.* **1943**, *150*, 140–167. [CrossRef]
3. Bland, D.R.; Ford, H. The calculation of roll force and torque in cold strip rolling with tensions. *Proc. Inst. Mech. Eng.* **1948**, *159*, 144–163. [CrossRef]
4. Bland, D.R.; Ford, H. Cold rolling with strip tension—Part III: An approximate treatment of the elastic com pression of the strip in cold rolling. *J. Iron Steel Inst.* **1952**, *171*, 245–249.
5. Sims, R.B. Calculation of roll force and torque in cold rolling by graphical and experimental methods. *J. Iron Steel Inst.* **1954**, *178*, 19–34.
6. Sims, R.B. Calculation of roll force and torque in hot rolling mills. *Proc. Inst. Mech. Eng.* **1954**, *168*, 191–200. [CrossRef]
7. Ford, H.; Ellis, F.; Bland, D.R. Cold rolling with strip tension—Part I: A new approximate method of calculation and a comparison with other methods. *J. Iron Steel Inst.* **1951**, *168*, 57–72.
8. Bland, D.R.; Sims, R.B. A note on the theory of rolling with tensions. *Proc. Inst. Mech. Eng.* **1953**, *167*, 371–372. [CrossRef]
9. Venter, R.; Abd-Rabbo, A. Modeling of the rolling process—I. *Int. J. Mech. Sci.* **1980**, *22*, 83–92. [CrossRef]
10. Freshwater, I.J. Simplified theories of at rolling—I: The calculation of roll pressure, roll force and roll torque. *Int. J. Mech. Sci.* **1996**, *38*, 633–648.
11. Alexander, J.M. On the theory of rolling. *Proc. R. Soc. Lond. A* **1972**, *326*, 535–555. [CrossRef]
12. Tlusty, J.; Critchley, S.; Paton, D. Chatter in cold rolling. *Ann. CIRP* **1982**, *31*, 195–199. [CrossRef]
13. Yun, I.S. Chatter in Rolling. Ph.D. Thesis, Northwestern University, Evanston, IL, USA, 1995.
14. Yun, I.S.; Wilson, W.R.D.; Ehmann, K.F. Chatter in the strip rolling process, Part I: Dynamic model of rolling. *Trans. ASME J. Manuf. Sci. Eng.* **1998**, *120*, 330–336. [CrossRef]
15. Yun, I.S.; Wilson, W.R.D.; Ehmann, K.F.; Wilson, W.R.D. Chatter in the strip rolling process, Part II: Dynamic rolling experiments. *Trans. ASME J. Manuf. Sci. Eng.* **1998**, *120*, 337–342. [CrossRef]
16. Yun, I.S.; Wilson, W.R.D.; Ehmann, K.F.; Wilson, W.R.D. Chatter in the strip rolling process, Part III: Chatter model. *Trans. ASME J. Manuf. Sci. Eng.* **1998**, *120*, 343–348. [CrossRef]
17. Yun, I.S.; Wilson, W.R.D.; Ehmann, K.F. Review of chatter studies in cold rolling. *Int. J. Mach. Tools Manuf.* **1998**, *38*, 1499–1530. [CrossRef]
18. Tamiya, T.; Furui, K.; Iida, H. Analysis of chattering phenomenon in cold rolling. In Proceedings of the International Conference on Steel Rolling, Tokyo, Japan, 29 September–4 October 1980; Iron and Steel Institute of Japan: Tokyo, Japan, 1980; pp. 1191–1202.
19. Hu, P.-H.; Ehmann, K.F. A dynamic model of the rolling process. Part I: Homogeneous model. *Int. J. Mach. Tools Manuf.* **2000**, *40*, 21–31. [CrossRef]
20. Kimura, Y.; Sondani, Y.; Nishiura, N.; Ikeuchi, N.; Mihara, Y. Analysis of Chatter in Tandem Cold Rolling Mills. *ISIJ Int.* **2003**, *43*, 77–84. [CrossRef]
21. Choudhary, A.K.; Gujre, V.S.; Verma, R.K. A Review on Chatter Analysis in Cold Rolling process. *Juniper Online J. Mater. Sci.* **2017**, *2*, 1–6.
22. Usmani, N.I.; Kumar, S.; Velisatti, S.; Tiwari, P.K.; Mishra, S.K.; Patnaik, U.S. Chatter detection using principal component analysis in cold rolling mill. *Diagnostyka* **2018**, *19*, 73–81. [CrossRef]
23. Wang, L.; Zhao, Y.; Zhu, Q.; Liu, Y.; Han, Q. Nonlinear Vibration Characteristic Analysis of Roller-Plate System Based on Asymptotic Methods. *ISIJ Int.* **2020**, *60*, 1237–1244. [CrossRef]
24. Cao, L.; Li, X.; Wang, Q.; Zhang, D. Vibration analysis and numerical simulation of rolling interface during cold rolling with unsteady lubrication. *Tribol. Int.* **2021**, *153*, 106604. [CrossRef]
25. Lu, X.; Sun, J.; Li, G.; Wang, Q.; Zhang, D. Dynamic analysis of vibration stability in tandem cold rolling mill. *J. Mech. Work. Technol.* **2019**, *272*, 47–57. [CrossRef]
26. Lu, X.; Sun, J.; Li, G.; Wang, Z.; Zhang, D. Stability Analysis of a Nonlinear Coupled Vibration Model in a Tandem Cold Rolling Mill. *Shock Vib.* **2019**, *2019*, 4358631. [CrossRef]
27. Liu, X.; Zang, Y.; Gao, Z.; Zeng, L. Time Delay Effect on Regenerative Chatter in Tandem Rolling Mills. *Shock Vib.* **2016**, *2016*, 4025650. [CrossRef]
28. Gao, Z.; Tian, B.; Liu, Y.; Zhang, L.-Y.; Liao, M. Dynamics-based optimization of rolling schedule aiming at dual goals of chatter suppression and speed increase for a 5-stand cold tandem rolling mill. *J. Iron Steel Res. Int.* **2021**, *28*, 168–180. [CrossRef]
29. Lu, X.; Sun, J.; Wei, Z.; Li, G.; Zhang, D. Effect of minimum friction coefficient on vibration stability in cold rolling mill. *Tribol. Int.* **2021**, *159*, 106958. [CrossRef]
30. Kopp, R.; Wiegels, H. *Einführung in die Umformtechnik*; Verlag der Augustinus Buchhandlung: Aachen, Germany, 1998.
31. McConnell, C.; Lenard, J.G. Friction in cold rolling of a low carbon steel with lubricants. *J. Mater. Process. Technol.* **2000**, *99*, 86–93. [CrossRef]

32. Tieu, A.K.; You, C.; Zhu, H.T.; Lu, C.; Jiang, Z.Y.; D'Alessio, G. Material Resistance and Friction in Cold Rolling. In Proceedings of the 6th World Congresses of Structural and Multidisciplinary Optimization, Rio de Janeiro, Brazil, 30 May–3 June 2005.
33. Zhao, H. Regenerative Chatter in Cold Rolling. Ph.D. Dissertation, Northwestern University, Evanston, IL, USA, 2008.
34. Yarita, I.; Furukawa, K.; Seino, Y.; Takimoto, T.; Nakzato, Y.; Nakagawa, K. An analysis of chattering in cold rolling of ultrathin gauge steel strip. *Trans. Iron Steel Inst. Jpn.* **1978**, *18*, 1–10. [CrossRef]
35. Hu, P.-H.; Zhao, H.; Ehmann, K.F. Third-octave-mode chatter in rolling. Part 1: Chatter model. *Proc. Inst. Mech. Eng. Part B J. Eng. Manuf.* **2006**, *220*, 1267–1277. [CrossRef]
36. Hu, P.-H.; Zhao, H.; Ehmann, K.F. Third-octave-mode chatter in rolling. Part 2: Stability of a single-stand mill. *Proc. Inst. Mech. Eng. Part B J. Eng. Manuf.* **2006**, *220*, 1279–1292. [CrossRef]
37. Hu, P.-H.; Zhao, H.; Ehmann, K.F. Third-octave-mode chatter in rolling. Part 3: Stability of a multi-stand mill. *Proc. Inst. Mech. Eng. Part B J. Eng. Manuf.* **2006**, *220*, 1293–1303. [CrossRef]